ELSEVIER

Journal of Applied Geophysics 46 (2001) 159–174

JOURNAL OF APPLIED GEOPHYSICS

www.elsevier.nl/locate/jappgeo

The complete gravity gradient tensor derived from the vertical component of gravity: a Fourier transform technique

Kevin L. Mickus [a,*], Juan Homero Hinojosa [b]

[a] *Department of Geosciences, Southwest Missouri State University, Springfield, MO 65804, USA*
[b] *College of Science and Technology, Texas A&M International University, Laredo, TX 78041, USA*

Received 23 February 2000; accepted 27 November 2000

Abstract

A technique has been to developed to determine the complete gravity gradient tensor from pre-existing vertical gravity data using the fast Fourier Transform (FFT). Since direct measurement of the entire gravity gradient tensor is generally unavailable, our technique provides an alternative determination of the gravity gradient tensor components. Traditionally, derivatives of vertical gravity ($g_{z,x}$, $g_{z,y}$, and $g_{z,z}$) have been the only gravity gradient tensor components that have been computed directly. Gravity gradient tensor components are computed for four different, three-dimensional (3-D), idealized horst-and-graben models, with varying depths to the horst. Comparing the FFT results with calculated gradient components from the 3-D models shows that the RMS error for each component, between the two results, is at most $\sim$3.3 Eötvos Units. In addition, measured gravity gradient components from an airborne survey over the Wichita Uplift and Anadarko Basin region of southwest Oklahoma compare favorably with the FFT-derived results using available vertical gravity data. No error analysis was attempted between the two results due to a low signal-to-noise ratio in the measured data. Our technique offers a novel way to transform and visualize the available data, and it also offers an inexpensive and previously unavailable subsurface mapping capability. © 2001 Published by Elsevier Science B.V.

Keywords: Gravity; Gradiometry; Fourier transform; Tensor

1. Introduction

Traditionally, the vertical component of the gravity field has been the only component measured because of the ease of obtaining these measurements and interpreting the data. On the other hand, to measure the gravity gradient tensor, a torsion balance had to be utilized, which was difficult to use, while the resulting data were also more difficult for geoscientists to understand (Bell, 1998). However, the importance and usefulness of the gravity gradient tensor (especially the vertical and horizontal gradients of vertical gravity) in locating subsurface objects have long been noted (Evjen, 1936; Hammer and Anzoleaga, 1975; Butler, 1983). Recent developments in aerial gradiometry systems (Jekely, 1988; Vasco, 1989; Bell et al., 1997) have resulted in a renewed interest in gravity gradient measurements, especially in the delineation of salt intrusions (Bell, 1998). However, these systems are not readily available and, for the most part, the data are proprietary,

* Corresponding author. Fax: +1-417-836-6006.
E-mail addresses: klm983f@smsu.edu, mickus@cart1.smsu.edu (K.L. Mickus).

0926-9851/01/$ - see front matter © 2001 Published by Elsevier Science B.V.
PII: S0926-9851(01)00031-3

which have limited the application of gravity gradiometry.

Because derivatives of vertical gravity have greater spatial resolution, delineate lateral boundaries of bodies better, and can provide more depth information than vertical gravity alone, numerous investigators (Evjen, 1936; Hammer and Anzoleaga, 1975; Stanley and Green, 1976; Butler, 1983; Blakely and Simpson, 1986; Grauch and Cordell, 1987; Butler, 1995) have derived theoretical expressions for the horizontal and vertical derivatives of the vertical gravity field resulting from simple geometries (spheres, horizontal cylinders, plates, truncated plates). Nevertheless, there has not been a complete analysis of all the components of the gravity gradient tensor. The most complete gravity gradient tensor analyses have been by Vasco (1989) and Vasco and Taylor (1991), who inverted gravity gradient tensor data collected by the Gravity Gradient Survey System (GGSS) developed by the United States Air Force (Jekely, 1988) for a three-dimensional (3-D) subsurface density structure in southwestern Oklahoma, and by Montana et al. (1992) who showed the differences in anomaly patterns for each tensor component due to a buried prism. Despite data quality problems of the then newly developed GGSS, the analysis by Vasco and Taylor (1991) showed that the gravity gradient components provided better resolution of basin depths than vertical gravity. However, no comparison between the individual gravity gradient components were given. Improvements in the GGSS have allowed for continued development of gravity gradiometry (Bell et al., 1997; Bell, 1998; Pratson et al., 1998) and its potential use in hydrocarbon exploration, where Pratson et al. (1998) showed how gravity gradient data provided an improved delineation of buried salt structures in the Gulf of Mexico.

In this study, we will first derive the gravity gradient tensor components as functions of the vertical component of gravity in the Fourier transform domain. Gunn (1974) was the first to apply the fast Fourier transform (FFT) to calculate certain gravity gradient components, and showed how to determine the vertical and horizontal gradients of vertical gravity. In a related study, Lourenco and Morrison (1971) applied the FFT to calculate the individual magnetic field components from total-field magnetic measurements. However, the FFT has not been applied to the complete gravity gradient tensor. The FFT-derived gravity gradient tensor components are compared to theoretical gravity gradient components computed from a horst-and-graben model using a 3-D forward modeling algorithm (Montana et al., 1992) to illustrate the usefulness of our technique and to interpret various gravity gradient tensor components. Finally, FFT-derived gravity gradient components are compared to measured gravity gradient components (Vasco, 1989; Vasco and Taylor, 1991) from the Wichita Uplift and Anadarko Basin region of southwestern Oklahoma.

2. Theory

Consider the gravity vector in free space, $\boldsymbol{g}(x,y,z) = (g_x(x,y,z),\ g_y(x,y,z),\ g_z(x,y,z))$, as three continuous and differentiable functions of three real variables. Further, consider the vertical component of $\boldsymbol{g}$ (g_z) measured on a horizontal surface in the (x,y)-plane at $z = z_o$, and given as $g_z(x,y,z_o)$. Since $\boldsymbol{g} = -\nabla\phi$, where $\phi = \phi(x,y,z)$ is the gravitational potential (a scalar function), it follows that $\nabla \cdot \boldsymbol{g} = \nabla \times \boldsymbol{g} = 0$. In addition, since the potential ϕ is a harmonic function satisfying Laplace's equation, $\nabla^2\phi = 0$, we have $(k_x^2 + k_y^2 + k_z^2)\ \Phi(\boldsymbol{k}) = 0$, in the Fourier transform domain for Laplace's equation, where $\Phi(\boldsymbol{k})$ is the Fourier transform of $\phi(x,y,z)$, $\boldsymbol{k}$ is the wavenumber vector $(k_x,\ k_y,\ k_z)$, and k_x, k_y, k_z are the wavenumbers in the x-, y-, and z-directions, respectively. The wavenumber k_z may be expressed in terms of the in-plane wavenumbers k_x, k_y (e.g., Blakely, 1996)

$$-ik_z = |\mathbf{k}|, \text{where } |\mathbf{k}| = \left(k_x^2 + k_y^2\right)^{1/2}.$$

From $\nabla \times \boldsymbol{g} = 0$, we obtain the following Fourier transform pairs:

$$\begin{aligned}
&\frac{\partial g_z}{\partial y} = \frac{\partial g_y}{\partial z} \Leftrightarrow \left(-ik_y\right)G_z = |\mathbf{k}|G_y \\
&\frac{\partial g_x}{\partial z} = \frac{\partial g_z}{\partial x} \Leftrightarrow |\mathbf{k}|G_x = \left(-ik_x\right)G_x \\
&\frac{\partial g_y}{\partial x} = \frac{\partial g_x}{\partial y} \Leftrightarrow \left(-ik_x\right)G_y = \left(-ik_y\right)G_x
\end{aligned} \tag{1}$$

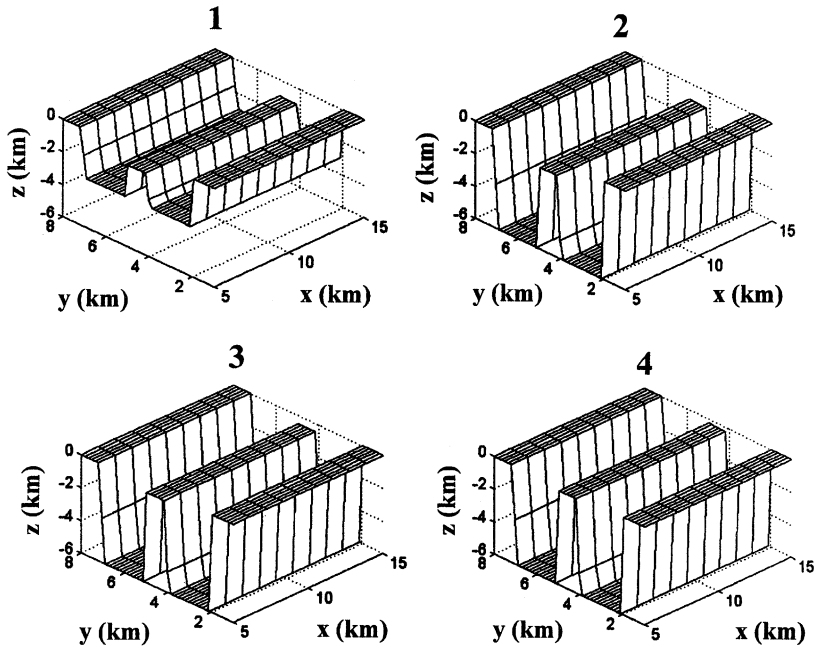

Fig. 1. Horst-and-graben models 1–4 used to calculate the vertical gravity values and gravity gradient tensor. The density contrast between the graben fill and the surrounding material is -0.2 g/cm^3 for all models.

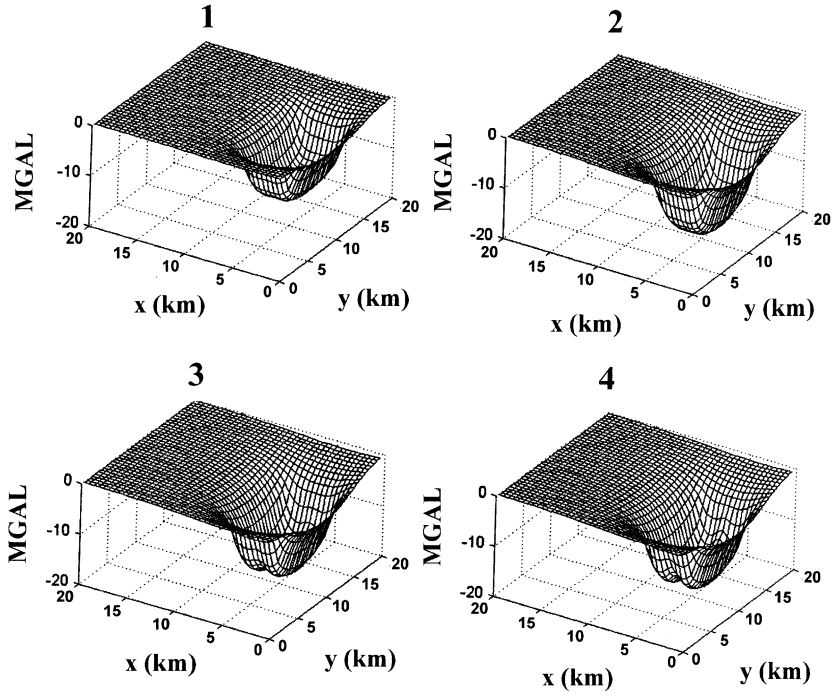

Fig. 2. Vertical gravity values for the models (1–4) shown in Fig. 1.

where g_x, g_y, g_z are the orthogonal components of $\boldsymbol{g}$, and $G_x = G_x(k_x,k_y)$, $G_y = G_y(k_x,k_y)$, $G_z = G_z(k_x,k_y)$ are the two-dimensional (2-D) Fourier transforms of g_x, g_y, g_z, respectively. From Eq. (1), we can obtain the Fourier transform of the gravity vector as follows:

$$g_x \Leftrightarrow G_x = \frac{(-ik_x)}{|\mathbf{k}|} G_z$$

$$g_y \Leftrightarrow G_y = \frac{(-ik_y)}{|\mathbf{k}|} G_z \tag{2}$$

$$g_z \Leftrightarrow G_z.$$

The gravity gradients are given as $g_{i,j}(\boldsymbol{x}) = \nabla \boldsymbol{g}(\boldsymbol{x})$, where $\boldsymbol{x} = (x,y)$, $g_{x,x} = \partial g_x/\partial x$, $g_{x,y} = \partial g_x/\partial y$, etc., which are the components of the gravity gradient tensor. A simple extension of the rela-

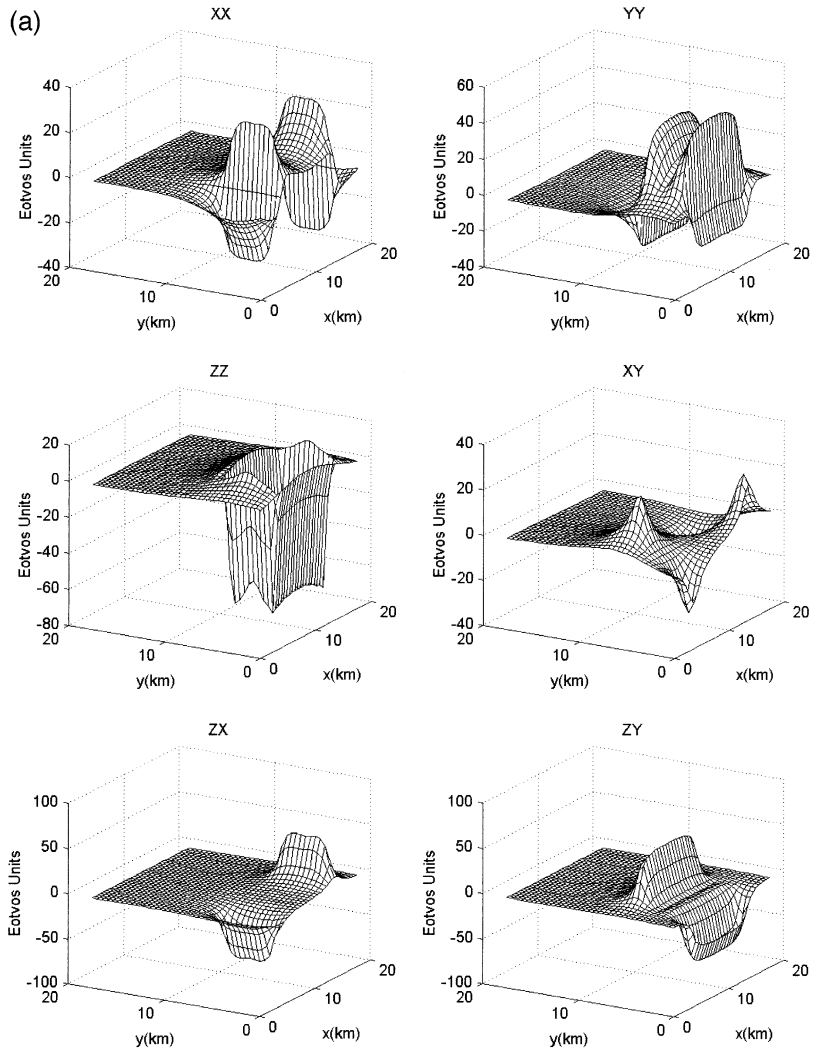

Fig. 3. (a) FFT-derived gravity gradient tensor components computed using the vertical gravity values determined from model 1 of Fig. 1. (b) FFT-derived gravity gradient tensor components computed using the vertical gravity values determined from model 2 of Fig. 1. (c) FFT-derived gravity gradient tensor components computed using the vertical gravity values determined from model 3 of Fig. 1. (d) FFT-derived gravity gradient tensor components computed using the vertical gravity values determined from model 4 of Fig. 1.

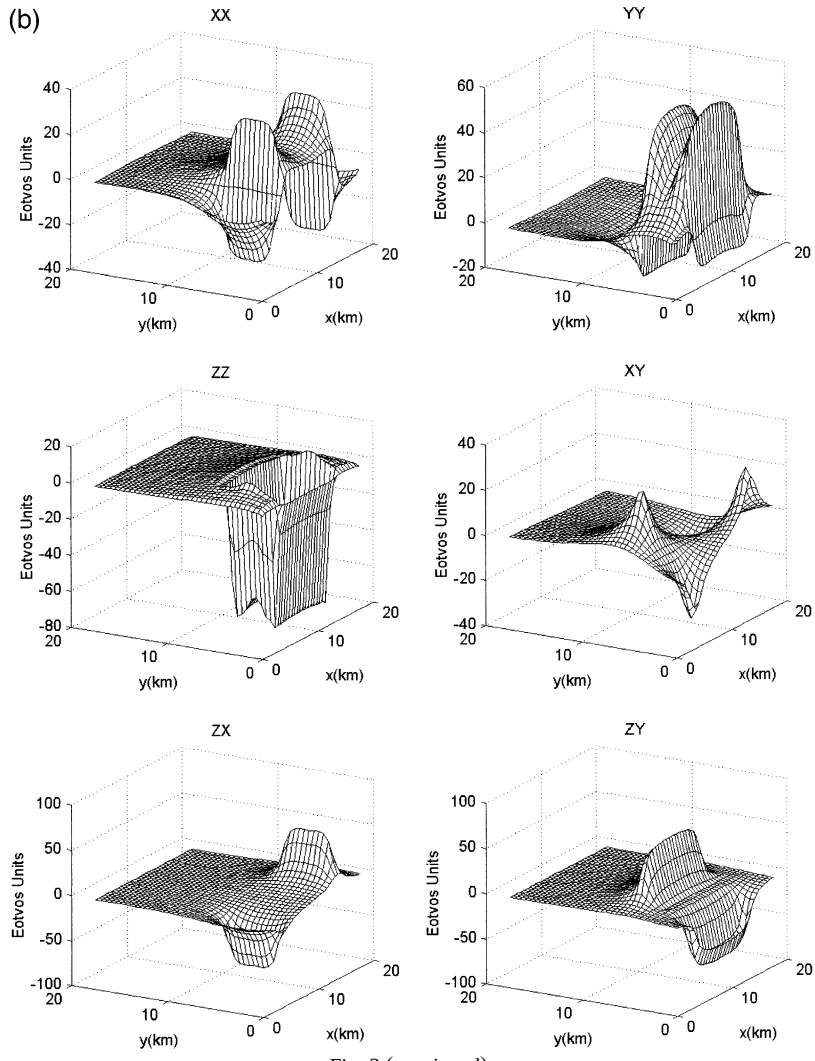

Fig. 3 (*continued*).

tions given above yields an expression for the complete gravity gradient tensor (Γ_{ij}) as follows:

$$\Gamma_{ij} = \mathcal{F}^{-1}\{[K(\mathbf{k})]G_z(\mathbf{k})\} \tag{3}$$

where

$$[K(\mathbf{k})] = \begin{bmatrix} \dfrac{-k_x^2}{|\mathbf{k}|} & \dfrac{-k_x k_y}{|\mathbf{k}|} & -ik_x \\ \dfrac{-k_x k_y}{|\mathbf{k}|} & \dfrac{-k_y^2}{|\mathbf{k}|} & -ik_y \\ -ik_x & -ik_y & |\mathbf{k}| \end{bmatrix} \tag{4}$$

with $|\mathbf{k}| \neq 0$, $i = x, y, z$, $j = x, y, z$, and with $\mathcal{F}^{-1}$ denoting the inverse Fourier transform operation.

It is clear from Eqs. (3) and (4) that the complete gravity gradient tensor may be computed from knowledge of only the vertical component of gravity. Furthermore, the researcher has the option of using either the free-air gravity anomaly or the Bouguer gravity anomaly when computing the gravity gradient tensor Γ_{ij}, and must have prior knowledge of this choice before meaningful interpretations of the data may be made. If the free-air gravity anomaly is used, the resulting Γ_{ij}, of course, represents the integrated

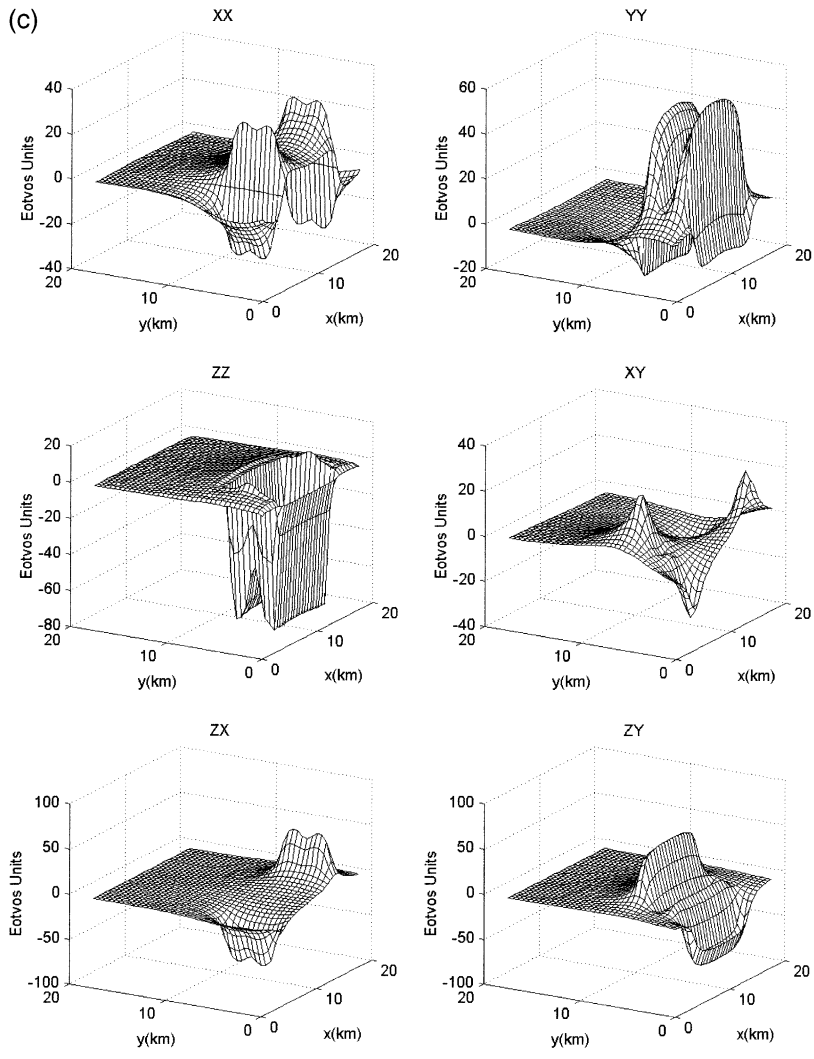

Fig. 3 (*continued*).

gravitational effect of both the surface and subsurface density anomalies. If, on the other hand, the Bouguer gravity anomaly is used, Γ_{ij} represents only the subsurface density anomalies, making the interpretation process more direct.

3. Examples and discussion

3.1. Idealized horst-and-graben models

To illustrate the above technique, gravity gradient tensor components produced by four different 3-D horst-and-graben models (Fig. 1) were constructed using a forward-modeling algorithm (Montana et al., 1992). Four models were used to both (i) illustrate our technique, and (ii) show the sensitivity of the different gravity gradient tensor components to small variations in subsurface features. We first calculated vertical gravity values for each of the four models (Fig. 2). These values were then used to determine the FFT-derived gravity gradient tensor components (Fig. 3a–d). The FFT-derived gradient components were then compared with the theoretically derived components (Fig. 4a–d) calculated from the 3-D forward modeling algorithm (Montana et al., 1992).

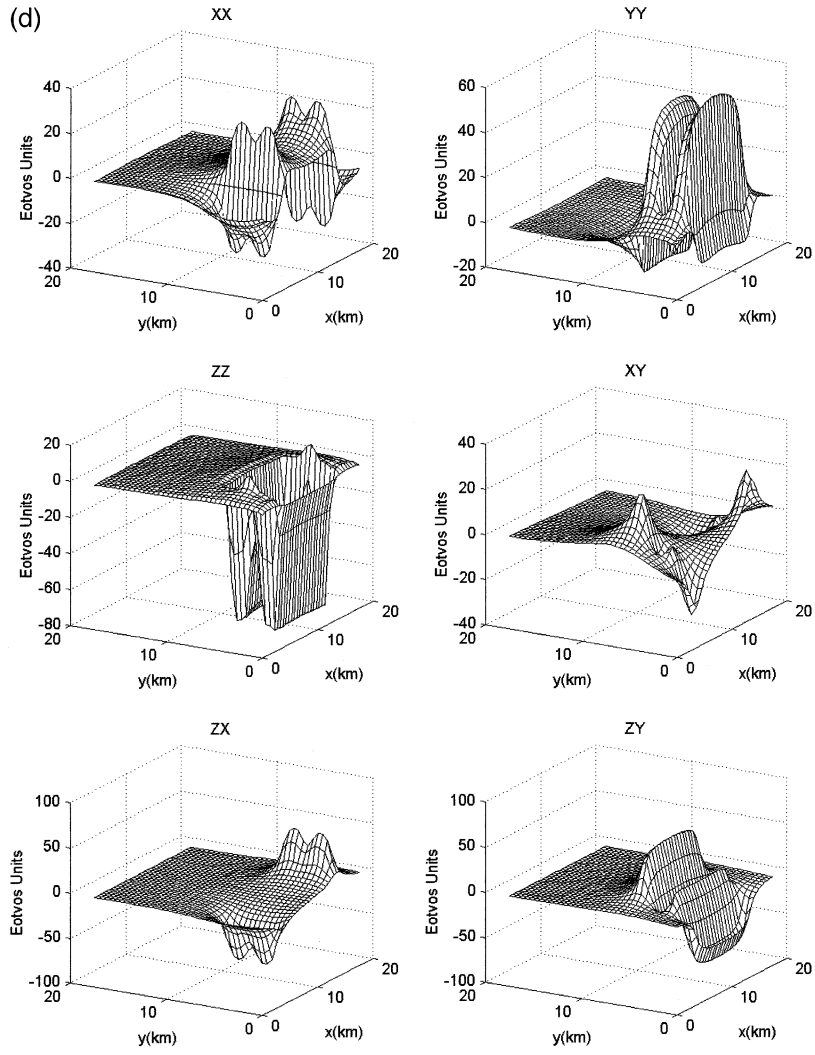

Fig. 3 (*continued*).

It can be seen that the FFT-derived and theoretically derived gradient components are almost identical, with only slight differences in amplitude. These differences are discussed in the next section.

3.2. Error analysis

The algorithm presented in this paper for computing the complete gravity gradient tensor involves the use of the FFT. We have quantified the error associated with the application of this technique by using the standard L_2-norm error estimate, or RMS error, e_{ij}, as follows:

$$e_{ij} = \sqrt{\frac{1}{MN}\sum_{m=1}^{M}\sum_{n=1}^{N}\left|g_{i,j}^{\mathrm{FFT}}(m,n) - g_{i,j}^{\mathrm{Mod}}(m,n)\right|^2} \tag{5}$$

where $g_{i,j}^{\mathrm{FFT}}(m,n)$ is the FFT gravity gradient tensor ijth-component, $g_{i,j}^{\mathrm{Mod}}(m,n)$ is the forward-model gravity gradient tensor ijth-component, M, N are the number of rows and columns, respectively, in the

2-D data array, and $i = x, y, z$, $j = x, y, z$. Table 1 shows the RMS error, e_{ij}, for the four models outlined above. The RMS errors obtained in this study range from a minimum of 0.3 Eötvos Units (E.U.) for the $g_{x,x}$ components, to a maximum of 3.3 E.U. for the $g_{z,y}$ components.

In addition, in order to visualize the difference between the model- and FFT-derived gravity gradient tensor components, we have calculated the deviations, or differences, corresponding to each model. Fig. 5a–b shows the deviations corresponding to models 1 and 4, respectively. The histograms clearly show a clustering of deviations close to zero, implying a good match between the model- and FFT-derived gravity gradient tensor components.

By examining the gravity gradient tensor components produced in all four models, it can be seen that, as the horst becomes shallower (1-km depth for models 1 and 2, 0.5 km for model 3, and 0.25 km for model 4), the various gradient components can be

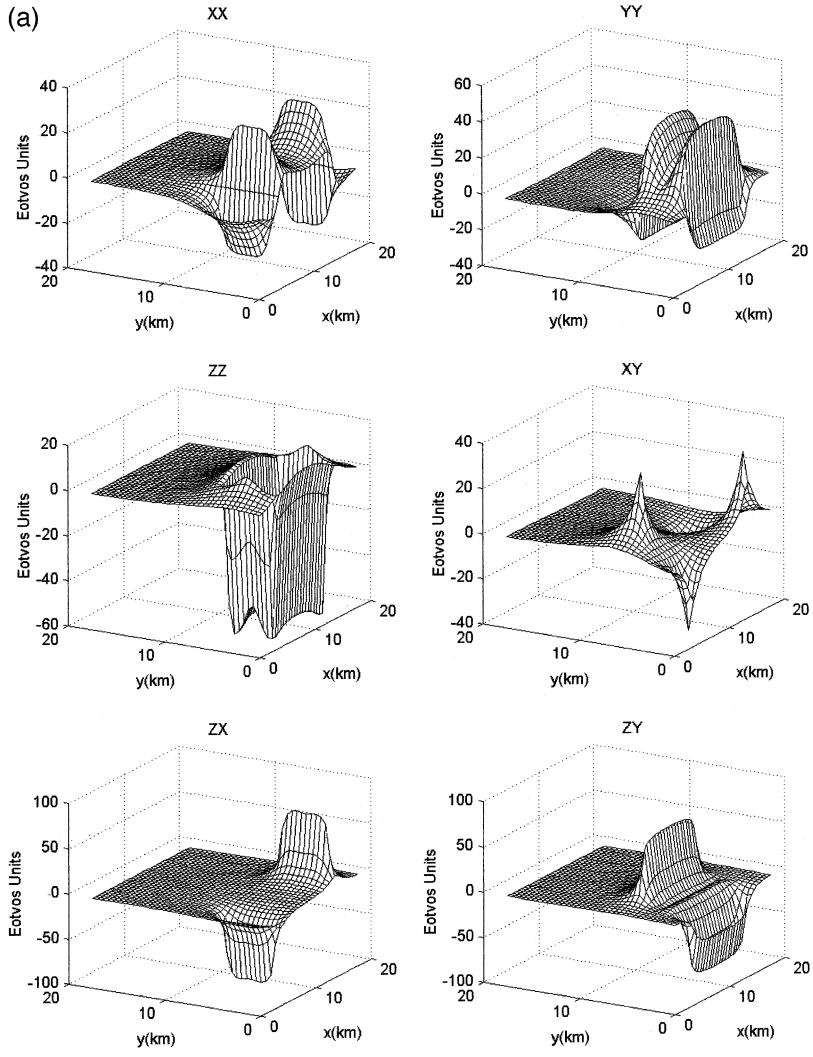

Fig. 4. (a) Calculated gravity gradient tensor components determined using model 1 of Fig. 1. (b) Calculated gravity gradient tensor components determined using model 2 of Fig. 1. (c) Calculated gravity gradient tensor components determined using model 3 of Fig. 1. (d) Calculated gravity gradient tensor components determined using model 4 of Fig. 1.

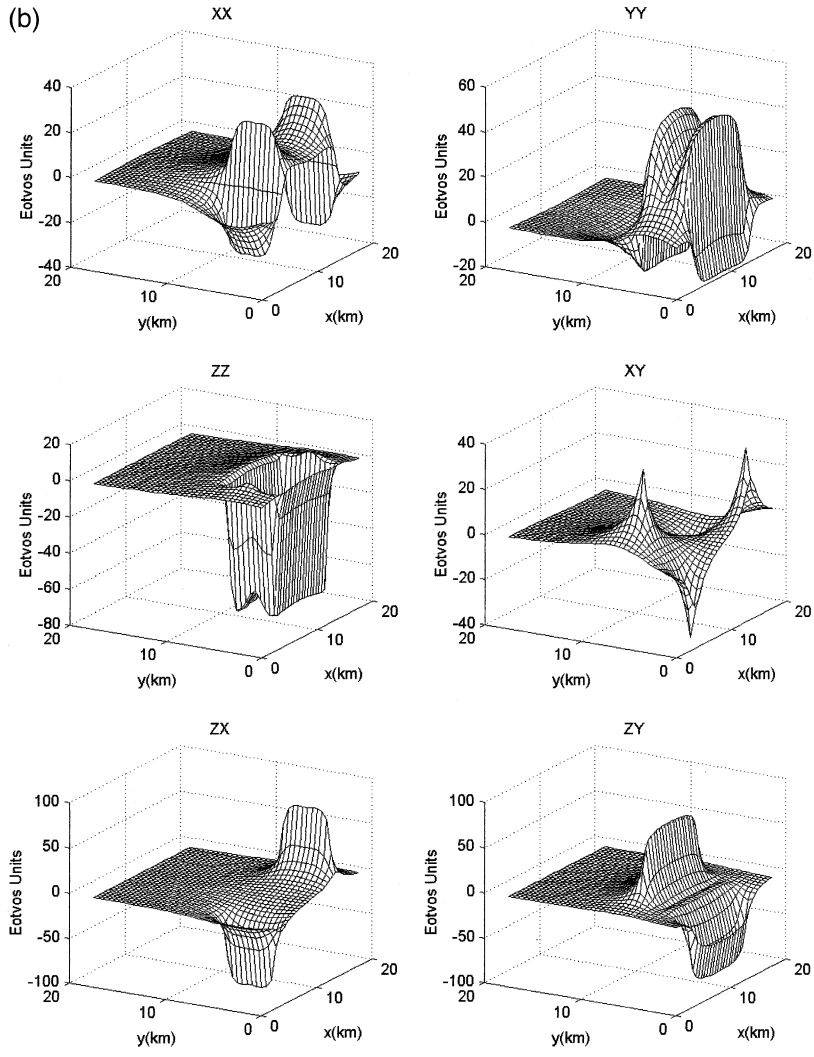

Fig. 4 (*continued*).

used to identify the exact subsurface location and horizontal dimensions of the horst (Figs. 3a–d and 4a–d). By using only g_z data (Fig. 2), anomalies due to the horst are not identifiable for models 1 and 2, while for models 3 and 4, there are noticeable anomalies of up to ~ 3 mGal in amplitude, which may be missed in actual data interpretation. However, each gradient component for models 3 and 4 reveals anomalies that allow the analyst to determine the exact location of the horst. The $g_{x,y}$ component is especially useful since it locates the corners of a subsurface mass anomaly. In these examples, the spikes (positive and negative) of the $g_{x,y}$ component locate the corners of the grabens (and horst, for shallow bodies ($\ll 0.5$ km)). For the deeper horst, these anomalies disappear, but the corners of the deeper grabens can still be determined. Also useful are the $g_{x,x}$ and $g_{y,y}$ components, which can be used to determine the location of the lateral boundaries of both the grabens and the horst. Anomalies due to the horst can be seen for models in the $g_{y,y}$ component, while only $g_{x,x}$ anomalies can be seen for models 1 and 2. If the horst were aligned parallel to the *y*-axis, the opposite would be true. Therefore,

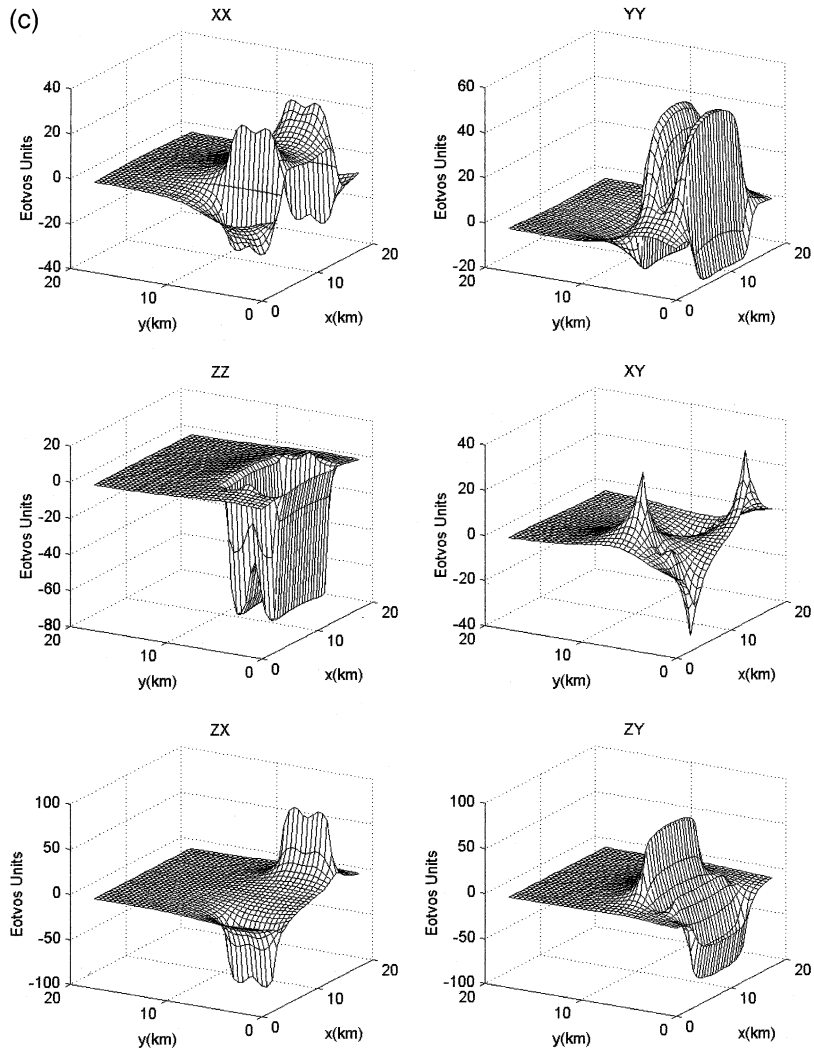

Fig. 4 (*continued*).

by making use of the entire gravity gradient tensor, the location of shallow subsurface structures is better delineated.

3.3. Earth data: southwestern Oklahoma

The only publicly available gravity gradient data set are the GGSS data collected in southwestern Oklahoma in the region of the Southern Oklahoma Aulacogen (Keller and Baldridge, 1995). This area contains up to 12–14 km of Cambrian rhyolites, granites, and gabbros that formed during early Paleozoic rifting along the southern margin of North America (Gilbert, 1983; Keller and Baldridge, 1995) and comprise the Wichita Uplift. These relatively dense igneous bodies are juxtaposed against the 9–11-km-deep Paleozoic Anadarko Basin to the north, and the 3–4-km-deep Hardeman Basin and an underlying unnamed Proterozoic basin (5–6-km thick) (Keller and Baldridge, 1995) to the south (Fig. 6). These tectonic features create one of the largest

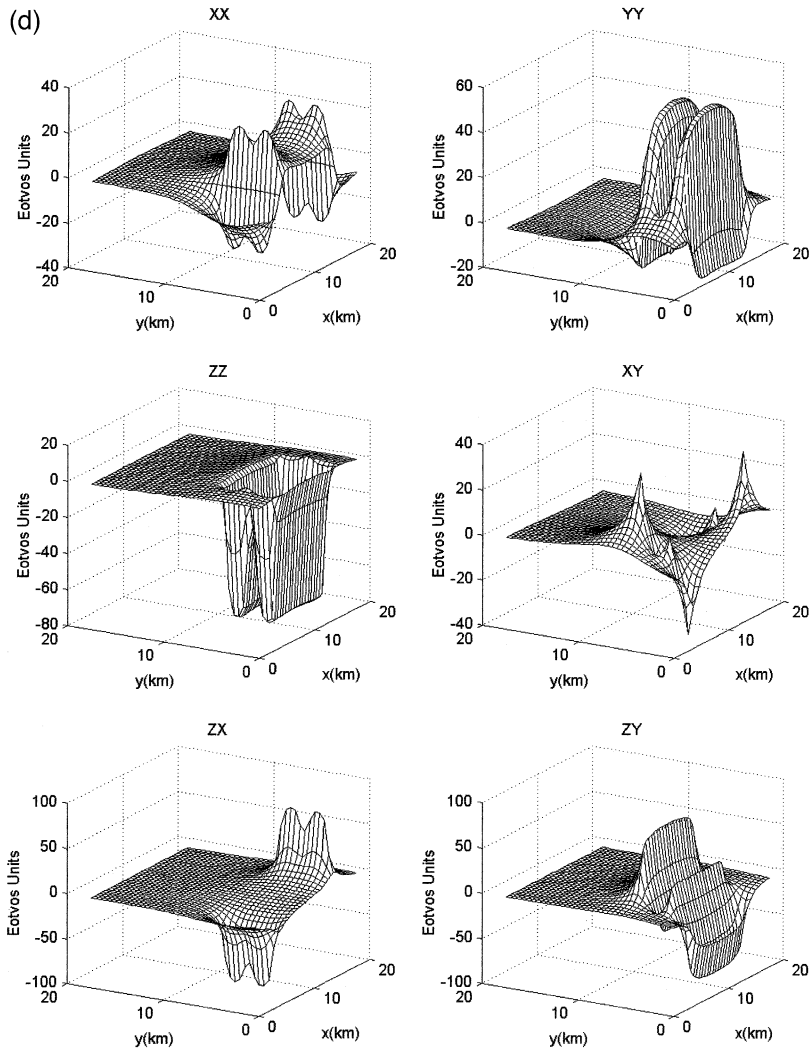

Fig. 4 (*continued*).

positive-amplitude gravity anomalies in the United States over the igneous intrusions, with gravity relative minima over the sedimentary basins (Fig. 6). These large-amplitude anomalies, with large vertical gravity gradients on relatively flat terrain, created an ideal location to test GGSS (Jekely, 1988). The relatively flat terrain lessened the effects of terrain-influenced anomalies, which have higher amplitudes in gravity gradient data as compared to vertical gravity data.

Table 1
RMS error between model and FFT gravity gradient tensor components

Gravity gradient tensor component	RMS error e_{ij} (E.U.) for each model			
	Model 1	Model 2	Model 3	Model 4
g_{xx}	0.3	0.5	0.5	0.5
g_{xy}	0.5	0.6	0.6	0.6
g_{yy}	1.3	1.8	1.8	1.8
g_{zx}	3.0	3.0	2.9	2.8
g_{zy}	2.9	2.9	2.9	3.3
g_{zz}	1.3	1.8	1.8	1.9

The resultant GGSS data set consisted of 30 north–south and 24 east–west tracks. The data were not of uniform quality, and the overall data quality was poor for many tracks (Vasco, 1989; Vasco and Taylor, 1991). Because of the poor data quality, we decided not to construct contour maps, and concen-

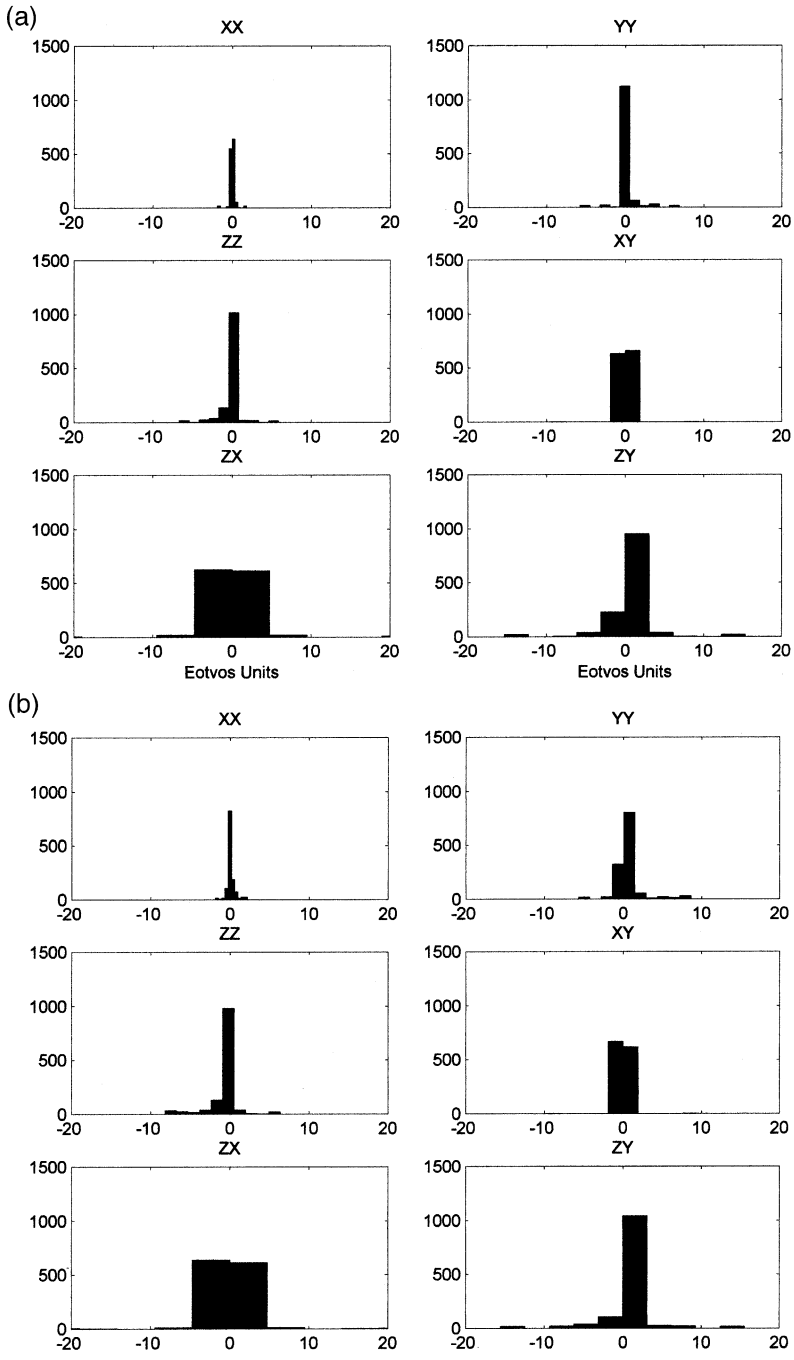

Fig. 5. (a) Histograms showing the deviations between the FFT-derived and model-calculated gravity gradient components from model 1. (b) Histograms showing the deviations between the FFT-derived and model-calculated gravity gradient components from model 4.

trated on a north–south track southwest of the exposed granites and rhyolites across the Wichita Uplift (Fig. 6). Additionally, the data set that we received did not contain the $g_{x,x}$ component, so this

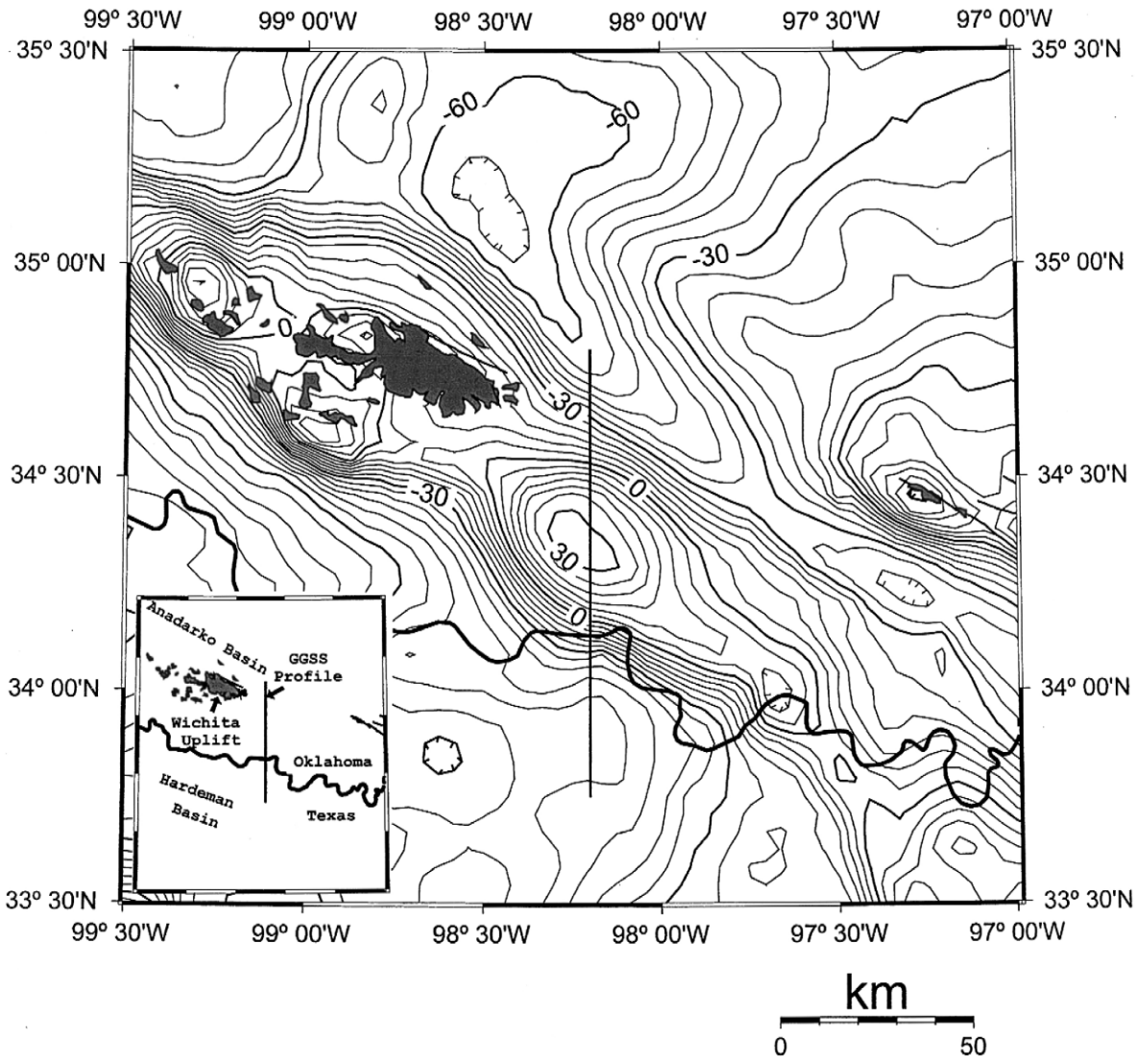

Fig. 6. Complete Bouguer gravity anomaly map of the Wichita Uplift and Anadarko Basin region. Shaded areas represent the exposed granites and gabbros of the Wichita Uplift. Thin lines represent major surface faults. The north–south thick line is the location of gravity gradient tensor values taken from a GGSS survey, which was compared with FFT-derived gravity gradient tensor components. The contour interval is 5 mGal and hachured contour lines represent gravity relative minima.

measured component was excluded from our analysis.

Figs. 7 and 8 show the measured and FFT-derived gravity gradient tensor components. Due to the low signal-to-noise ratio in the measured data, we did not perform an error analysis comparing the two data sets. Even with the high noise levels, the average trends of both data sets roughly agree. The profile crosses the Wichita Uplift (Fig. 6), which is associated with a ~35-mGal-gravity anomaly. Seismic refraction and gravity models (Keller and Baldridge, 1995) show that this anomaly is caused by a rectangular prism that extends to approximately 12–14 km in depth. Since this intrusion extends over 100 km to the northwest and at least 50 km to the southeast, the source body can be considered 2-D at the location of

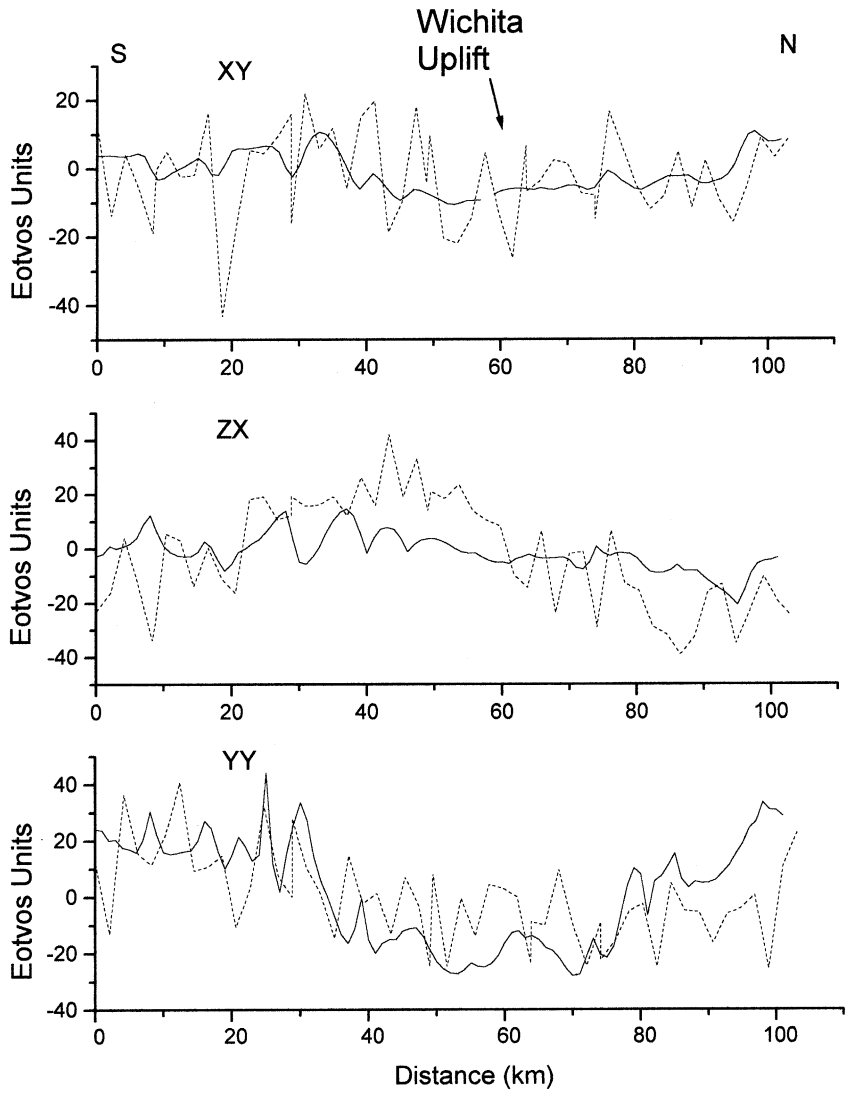

Fig. 7. Profiles comparing measured (dashed) and FFT-derived (solid) $g_{x,y}$, $g_{z,x}$ and $g_{y,y}$ values.

our profile. Gravity gradient signatures for such a body (rectangular prism) include $g_{x,x}$ and $g_{z,x}$ maximum at the boundaries, with a $g_{x,x}$ minimum in the body's center, $g_{y,y}$ and $g_{x,y}$ minima and a $g_{z,z}$ maximum over the body's center (Montana et al., 1992). This is seen for both the measured and derived gradient components (Figs. 7 and 8). Since the profile crosses far from the northwest and southeast edges of the body, the large amplitude anomalies associated with the $g_{x,y}$-components along the body's boundaries are not seen along the profile. However, there are small amplitude $g_{x,x}$, $g_{z,x}$, and $g_{x,y}$ anomalies at approximately 40 and 80–100 km, which result from the body being at an angle to the *x*-axis (east–west).

The gravity maximum due to the Wichita Uplift (Fig. 6), located at ~60 km along the profile, is best seen on the $g_{z,z}$ component as an "even-type" profile, i.e., symmetrical about a vertical axis crossing the center of the anomaly, with the north and south lateral boundaries of the Wichita Uplift being located at ~85–95 km and ~35–50 km, respectively. The

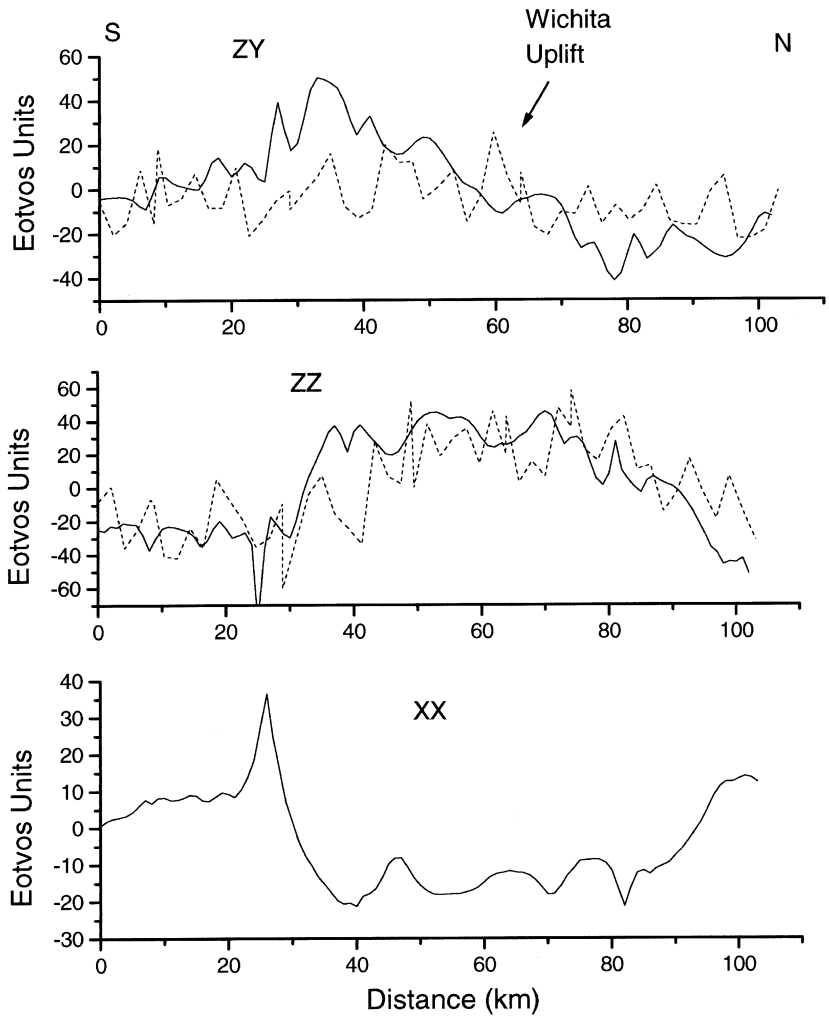

Fig. 8. Profiles comparing measured (dashed) and FFT-derived (solid) $g_{z,y}$ and $g_{z,z}$ values. The FFT-derived $g_{x,x}$ component is also shown for the sake of completeness. Note that the measured $g_{x,x}$ was not available to the authors.

$g_{y,y}$ profile also delineates the north and south lateral boundaries of the Wichita Uplift. Note also that the $g_{z,x}$ and $g_{z,y}$ profiles are "odd-type" profiles, and locate the Wichita Uplift maximum at the "inflection point" of the profiles, i.e., at $\sim$ 60 km along the profile.

4. Conclusions

A Fourier transform technique has been developed to calculate the complete gravity gradient tensor using vertical gravity data. Comparisons between FFT-derived gravity gradient tensor components and calculated values from a 3-D forward modeling program using a horst-and-graben model show that the RMS error between the two solutions is $<$ 3.5 E.U. for all components, and variations in the forward model. Different forward models, with varying depth to the top of the horst, indicate that using the entire gravity gradient tensor, especially the $g_{x,x}$, $g_{y,y}$ and $g_{x,y}$ components, will greatly increase the determination of the lateral boundaries of the horst-and-graben for top-of-horst depths of less than $\sim$ 0.5 km. Using

vertical gravity data from the Wichita Uplift and Anadarko Basin region of southwestern Oklahoma, gravity gradient profiles were computed and compared with measured components from an airborne survey. The two data sets agree in the general trends, but a low signal-to-noise ratio in the measured data prohibited an analysis of the error. Since the complete gravity gradient tensor is usually difficult to determine, and thus not readily available, the FFT-derived gravity gradient tensor components offer a novel way to visualize potential field data, and will increase the resolution for determining the location of subsurface structures. Our technique, however, does not replace the actual measurement of the gravity gradient tensor, but the low RMS errors achieved using this technique indicate that the FFT-derived gradients closely approximate the true gradients.

Acknowledgements

The authors wish to thank D.K. Butler and an anonymous reviewer for their suggestions on improving the manuscript.

References

Bell, R., 1998. Gravity gradiometry. Scientific American 278, 74–79.

Bell, R., Anderson, R., Pratson, L., 1997. Gravity gradiometry resurfaces. The Leading Edge 16, 55–60.

Blakely, R.J., 1996. Potential Theory in Gravity and Magnetic Applications. Cambridge Univ. Press, New York.

Blakely, R.J., Simpson, R.W., 1986. Locating edges of source bodies from magnetic or gravity anomalies. Geophysics 51, 1494–1498.

Butler, D.K., 1983. Microgravimetry and the theory, measurement, and application of gravity gradients. PhD Thesis, Texas A&M Univ., College Station, USA.

Butler, D.K., 1995. Generalized gravity gradient analysis for 2-D inversion. Geophysics 60, 1018–1028.

Evjen, H.M., 1936. The place of the vertical gradient in gravitational interpretations. Geophysics 1, 127–136.

Gilbert, C.M., 1983. Timing and chemistry of igneous events associated with the Southern Oklahoma Aulacogen. Tectonophysics 94, 439–455.

Grauch, V.J.S., Cordell, L., 1987. Limitations of determining density or magnetic boundaries from the horizontal gradient of gravity or pseudogravity data. Geophysics 52, 118–121.

Gunn, P.J., 1974. Linear transformations of gravity and magnetic fields. Geophysical Prospecting 23, 300–312.

Hammer, S., Anzoleaga, R., 1975. Exploring for stratigraphic traps with gravity gradients. Geophysics 40, 256–268.

Jekely, C., 1988. The gravity gradiometer survey system (GGSS). EOS Transactions of the American Geophysical Union 69, 116–117.

Keller, G.R., Baldridge, S.W., 1995. The Southern Oklahoma Aulacogen. In: Olsen, K. (Ed.), Continental Rifts. Elsevier, Amsterdam, pp. 427–436.

Lourenco, J.S., Morrison, H.F., 1971. Vector magnetic anomalies derived from measurements of a single component of the field. Geophysics 38, 359–368.

Montana, C., Mickus, K.L., Peeples, W.J., 1992. Program to calculate the gravitational field and gravity gradient tensor due to right rectangular prisms. Computers and Geosciences 18, 587–602.

Pratson, L.F. et al., 1998. Results from a high-resolution, 3-D marine gravity gradiometry survey over a salt structure, Mississippi Canyon area, Gulf of Mexico. In: Gibson, R., Millegan, P. (Eds.), Geological Applications of Gravity and Magnetics: Case Histories. American Association of Petroleum Geologists, Tulsa, OK, pp. 139–148.

Stanley, J.M., Green, R., 1976. Gravity gradients and interpretation of the truncated plate. Geophysics 41, 1370–1376.

Vasco, D.W., 1989. Resolution and variance operators of gravity and gravity gradiometry. Geophysics 54, 889–899.

Vasco, D.W., Taylor, C., 1991. Inversion of airborne gravity gradient data, southwestern Oklahoma. Geophysics 54, 90–101.